Dependence of the Dielectric Constant on the Fluorine Content and Porosity of Polyimides

Muhammad Bisyrul Hafi Othman, Nicholas Ang Soon Ming, Hazizan Md Akil, Zulkifli Ahmad

School of Materials and Mineral Resources Engineering, Engineering Campus, Universiti Sains Malaysia, Seri Ampangan, 14300 Nibong Tebal, Pulau Pinang, Malaysia

Received 30 May 2010; accepted 23 November 2010
DOI 10.1002/app.33837
Published online 11 April 2011 in Wiley Online Library (wileyonlinelibrary.com).

ABSTRACT: The trend toward miniaturization in integrated circuit fabrication demands good interlayer dielectric materials. This need can be met by polyimide (PI), which has extreme thermal and chemical stability and, most importantly, a low dielectric constant. Four porous PIs with symmetrically substituted fluorine contents were synthesized. Different porosity levels were achieved with a sol–gel technique through the incorporation of 10 or 20% tetraethyl orthosilicate into the polymer matrix and then acid etching. Their dielectric constants were correlated with the fluorine contents and porosity levels. High porosity levels and higher fluorine contents induced substantial decreases in the PI dielectric constants (2.4–2.7). The resultant values were within the applicable range for dielectric materials in integrated circuits. © 2011 Wiley Periodicals, Inc. J Appl Polym Sci 121: 3192–3200, 2011

Key words: dielectric properties; halogenated; polyimides

INTRODUCTION

The search for polymers to be used as dielectric materials for reducing resistance–capacitance (RC) time delays, cross-talk, and power dissipation in high-density and high-speed integrated circuits has been the focus of many researchers.[1–11] The excellent thermal and mechanical stability of polyimide (PI) has made it a natural choice as a low-dielectric material.[3–5] However, the dielectric constants of this polymer, which range from 3.4 to 2.8, are not sufficient for the demands of integrated circuit module miniaturization. Several techniques have been applied to produce low-dielectric-constant PIs; these include the production of porous materials and the incorporation of fluorine.[6,12] Void fabrication allows the diffusion of air into the polymer matrices; because air has a dielectric constant of 1, the dielectric constant is lowered. One method for inducing porosity in the PI structure involves the preparation of block copolymers consisting of thermally stable and thermally labile blocks, the latter being the dispersed phase.[13–15] Foam formation is then effected by the thermolysis of the thermally labile block, which leaves pores with sizes and shapes corresponding to the initial copolymer morphology.[6,12–14,16]

Several works have demonstrated that the incorporation of fluorine into PI effectively reduces the dielectric constant.[17–20] This is due to the small size and low polarizability of the fluorine atom, which otherwise readily allows electron orientation when it is exposed to an electric field. The dielectric constant can be determined with the Debye formulation:[21]

$$(\varepsilon_r - 1)/(\varepsilon_r + 2) = \rho P_m/M$$

where ε_r is permittivity (dielectric constant) of polymer, ρ is density of polymer. P_m is relative permittivity (dielectric constant) of polymer and M is the molar mass of polymer. From the value of P_m, it can be shown that the dielectric constant is dependent on the polarizability and dipole moments in the molecule under an applied field and on the density of the polymer. Hougham et al.[19] have shown that the nonsymmetrical substitution of fluorine for hydrogen increases the average magnitude of the dielectric constant by approximately 0.05 per substituted ring.[19] The symmetric substitution of fluorine does not induce the net dipole moment of the polymer and hence does not increase the dielectric constant. The decrease in the dielectric constant with symmetric fluorine substitution has been attributed to a combination of electronic polarizability and a larger free volume.

The poor processability of PIs is almost the only detrimental factor limiting their widespread application. This problem is due to the highly rigid and stiff chain backbone and the extensive interchain interactions. The glass transition sometimes is greater than 400°C, and the melting temperature exceeds the

Correspondence to: Z. Ahmad (zulkifli@eng.usm.my).
Contract grant sponsor: Science University of Malaysia; contract grant number: 6071003 (Fundamental Research Grant Scheme).

decomposition temperature. The appropriate starting monomers, chain flexibility, and interchain interactions can be tailored to yield PIs with moderate thermal properties.

This work reports the relationships of the fluorine content and pore density with the dielectric constant for a series of PIs with moderate thermal properties. They were synthesized through the use of monomers with flexible ether and saturated carbon–carbon bonds as bridging units in the chain backbone. The dianhydride moiety was deliberately chosen to avoid fused ring structures or sterically rigid bridges. The fluorine content in the PI series was monitored, and the level of porosity was subsequently controlled with the sol–gel method.[22–24] The latter was based on the methodology developed by Wen et al[23] and Sanchez et al.[24–25] The characterization of pure PI and porous PI was performed through a comparison of their dielectric constants, thermal properties, and surface morphology. The general synthesis routes for the production of PIs involved the use of dianhydride and dianiline to produce a poly(amic acid) (PAA) intermediate at room temperature. This PAA was then cured over 300°C to form PI thin films. We discuss the structure and properties (with respect to the fluorine content and porosity) and the dielectric constants of these PIs of moderate thermal stability.

EXPERIMENTAL

Materials

4,4′-(4,4′-Isopropylidenediphenyl-1,1′-diyldioxy)dianiline (BAPP), 4′,4‴-(hexafluoroisopropylidene) bis(4-phenoxyaniline) (BDFA), 4,4′-methylene dianiline (MDA), 4,4-(hexafluoroisopropylidene)diphthalic anhydride (6FDA), 3,3′,4,4′-biphenyl tetracarboxylic dianhydride (BPDA), and tetraethyl orthosilicate (TEOS) were obtained from Sigma–Aldrich Sdn. Bhd. They were used as received. *N,N*-Dimethylacetamide (DMAC, Kuala Lumpur, Malaysia), dimethylformamide, and hydrofluoric acid (HF, Kuala Lumpur, Malaysia) from Fluka were freshly refluxed over calcium hydride before they were used as solvents. Methanol, chloroform, acetone, and tetrahydrofuran (J. T Baker, Philipsburg, NJ) were freshly distilled before use, whereas sulfuric acid, HF, and toluene (Merck, Hohenbrunn, Germany) were used without any further purification.

Synthesis of the PI system

The PIs were produced with a general two-step synthesis: polyaddition followed by polycyclocondensation between a dianiline and a dianhydride of a tetracarboxylic acid.[10] The product was PAA; a subsequent thermal treatment induced chain crosslinking and yielded the PIs. The procedure was as follows (BAPP and BPDA are used as examples): BAPP (0.0092 mol, 3.78 g) was dissolved in freshly distilled DMAC (60 mL) in a three-necked, round-bottom flask with a 250-mL capacity that was equipped with a mechanical stirrer. After the complete dissolution of the dianiline, BPDA powder (0.0092 mol, 2.71 g) was subsequently introduced into the solution stepwise. The brownish, viscous mixture was mechanically stirred at room temperature for at least 1 h to allow polymerization to occur.

The viscous solution was poured into a 500-mL beaker filled with distilled water, and a white precipitate of PAA was produced. The solids were stirred and pressed with a glass rod to ensure complete precipitation. The distilled water was decanted, and the washing was repeated another 3 times. The PAA precipitate was then filtered off, and the solids were allowed to dry at room temperature for at least 24 h. The PAA solids were then further dried in an oven at 80°C *in vacuo.* Once they were entirely dried, they were stored in desiccators. The curing procedure that yielded the cured PIs involved the heating of the dried PAA solids at 80 (1 h), 150 (1 h), and 300°C (3 h) in a Thermolyne 48,000 muffle furnace (Durham, NC, USA). Four PIs were synthesized, and the chemical structures of the monomers are shown in Table I.

Preparation of the PAA/silica (SiO_2) mixture

The fabrication of this polymer into porous foam thin films involved the preparation of a PI/SiO_2 hybrid material via the sol–gel process with SiO_2 constituting the dispersed phase. The dried PAA solids (1–2 g) were dissolved in DMAC (1 g of PAA to 10 mL of DMAC). The mixture was stirred mechanically until all the PAA solids were dissolved. Then, a certain amount of TEOS (10 or 20%) was added to the PAA solution, and the mixture was further stirred for at least 6 h. The resultant hybrid samples were dried at 80°C (1 h), and this was followed by thermal curing at 150 (1 h), 200 (1 h), and 300°C (1 h). Thin films were obtained via spin coating at 3000 rpm for 30 s. The SiO_2 phase was subsequently etched away by HF, and this left pores whose size and shape were dictated by the SiO_2 particles. The preparative procedure is summarized in Figure 1.

Characterization

The inherent viscosity was determined with an Ubbelohde calibrated viscometer (Loughborough, England) tube according to ASTM D 2857 with 0.30 g of PI/dL. The hardness was measured with a Techlock GS (Munich, Germany) series durometer according to ASTM D 2240 at 23–25°C with a film thickness of 3.0 mm. The glass-transition

TABLE I
Monomers and Synthesized PI Series

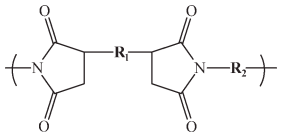

Polyimide	Dianhydride R_1	Dianiline R_2	Polyimide repeated unit
6 FDA-BDFA	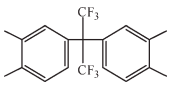	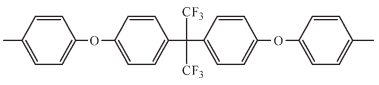	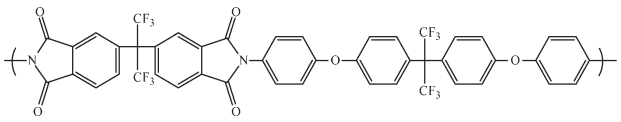
6 FDA-MDA	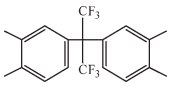	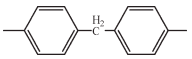	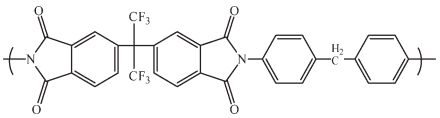
BPDA-BDFA	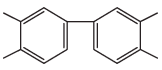	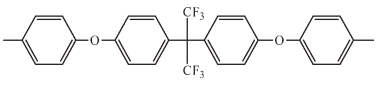	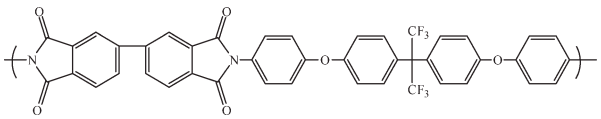
BPDA-BAPP	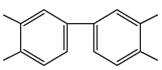	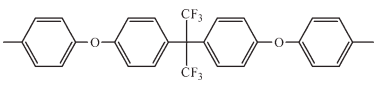	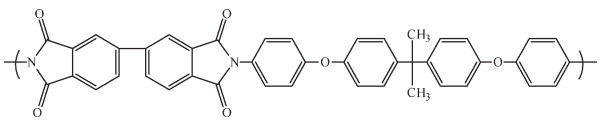

temperatures were determined with a PerkinElmer DSC-6 (Norwalk, CT, USA) analyzer according to ASTM D 3418 at a heating rate of 10°C/min in N_2 from 30 to 340°C. The thermal degradation temperature at a 5% weight loss was determined with a PerkinElmer Pyris 6 thermogravimetric analyzer according to ASTM E 1131 from 30 to 800°C at a heating rate of 10°C/min in N_2. The PI thin films were characterized with a Perkin Elmer Spectrum GX Fourier transform infrared (FTIR) instrument according to ASTM E 1252 in the wavelength range of 4000–600 cm^{-1}. Elemental analyses (carbon, hydrogen, and nitrogen) of pure BAPP–BPDA and BDFA–BPDA test specimens were performed on a PerkinElmer 2400 series II CHNS/O analyzer. Scanning electron microscopy (SEM) was performed with a Zeiss Supra (Oberkochen, Germany) 35VP field emission scanning electron microscope that also included an electron diffraction X-ray (EDX) analyzer. The latter was used to performed surface elemental analyses. The capacitance–voltage measurements (p-type) were performed on a Keithley model (Cleveland, OH, USA) 82 CV meter at a probing frequency of 1 MHz with an applied electric field ranging from −2 to 4 V at a ramping rate of −0.02 V/s on a metal–

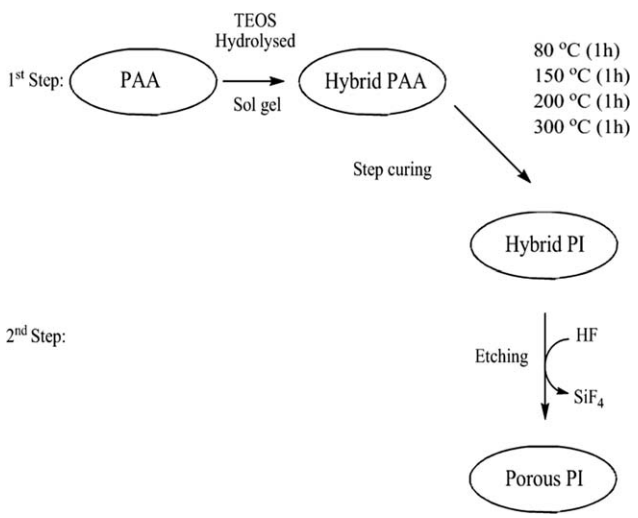

Figure 1 Preparation of a porous PI with the sol–gel method.

TABLE II
Char Yield, Inherent Viscosity, Hardness, and Thermal Properties of the PIs

PI	Inherent viscosity (dL/g)	Char yield (%)	Shore D hardness[b]		Glass-transition temperature (°C)[c]	Thermal degradation temperature at a 5% weight loss (°C)[c]	
			Pure	Porous		Pure	Porous
6FDA–BDFA	0.7160	51	47.8	45.0	268.3	523	515
6FDA–MDA	0.5523	56	62.0	50.3	—[d]	503	451
BPDA–BDFA	0.8875	52	—	—	260.7	539	524
BPDA–BAPP	1.0674	58	—	—	240.8	516	507

[a]Measured in DMAc at 25 + 0.1°C at a concentration of 0.3 g/dL.
[b] Measured according to ASTM D 2240.
[c] Measured at a heating rate 10°C/min.
[d] Undetectable.

insulator–semiconductor capacitor, and the resulting current flowing into the test structure was monitored. The film thickness was measured with a Zeiss atomic force microscope with an SIS Ultra objective. The films were desiccated overnight before the measurements at room temperature and a relative humidity of 25–35%.

RESULTS AND DISCUSSION

Synthesis considerations

The four PIs were synthesized as follows: stepwise polyaddition of the respective dianhydride and dianiline monomers to produce the PAA intermediate and then polycondensation with ring closure and elimination of water to produce the corresponding PIs.[10,26] Except for BAPP–BPDA, the PIs contained a symmetrically substituted fluorine substituent. Inherent viscosity measurements (0.55–1.07 dL/g) showed products with quite high molecular weights, and the char yields were approximately 51–58%. All the PIs, both pure and porous, displayed moderate thermal stability with glass-transition temperatures in the range of 240–269°C and thermal degradation temperatures (5% weight loss) in the range of 503–539°C. These results were within the ranges reported by Gosh and Mittal[10] and Mittal.[27] Furthermore, the moderate thermal stability was due largely to the presence of flexible ether bonds in 6FDA–BDFA and BPDA–BDFA. Because of their flexibility, the segmental motion was readily affected during the thermal treatment, which subsequently induced a lower glass transition. Additionally, the utilization of BPDA with a single bond adjoining the dianhydride moiety further induced the chain flexibility of the synthesized BPDA–BDFA and BPDA–BAPP. In the case of 6FDA–MDA, the methylene group bridging the two aromatic rings similarly induced chain flexibility. Certainly, several other factors (i.e., the structure, molecular mass, and chain interpenetration) jointly contributed to the lowering of the glass transition. However, the types of linkages present in these PIs contributed at least to some degree toward the lowering of the thermal stability. Table II summarizes the char yields, inherent viscosities, hardness values, and thermal properties of the PIs.

The proposed reaction mechanism for TEOS during sol–gel reactions is depicted in Figure 2 and is based on the work of Cornelius and Marand.[26] These reactions are typically catalyzed by an acid or a base. No water was added in this work because it was supplied during the *in situ* imidization of the intermediate PAA into PI. Because of the chain extension during the condensation step, micrometer-sized inorganic domains were generated with a homogeneous distribution within the PI matrix. The etching process was performed through the soaking of the materials in HF for 2 h. The completion of this process was confirmed by EDX spectroscopy, which revealed a complete absence of silicon in the cryogenically fractured surface (Figure 3).

FTIR was used to confirm the identity of the products, as shown in Figure 4. The representative FTIR spectrum of BAPP–BPDA showed a broad and strong peak in the region of 3500–3000 cm^{-1} [Fig. 4(a)], and this corresponded to the overlapping hydroxyl and secondary amine groups. The disappearance of these peaks implied complete imidization of PAA into the final PI products [Fig. 4(b)].[28–30] Moreover, there were two peaks corresponding to asymmetric imide C=O stretching (1774–1784 cm^{-1}) and symmetric imide C=O stretching (1717–1721 cm^{-1}).[28,30–32] In the BAPP–BPDA and 6FDA–MDA spectra, weak peaks in the range of 2900–2850 cm^{-1} were observed and correspond to the C—H bond of the methylene and methyl group. These peaks were noticeably absent in the 6FDA–BDFA and BDFA–BPDA spectra.

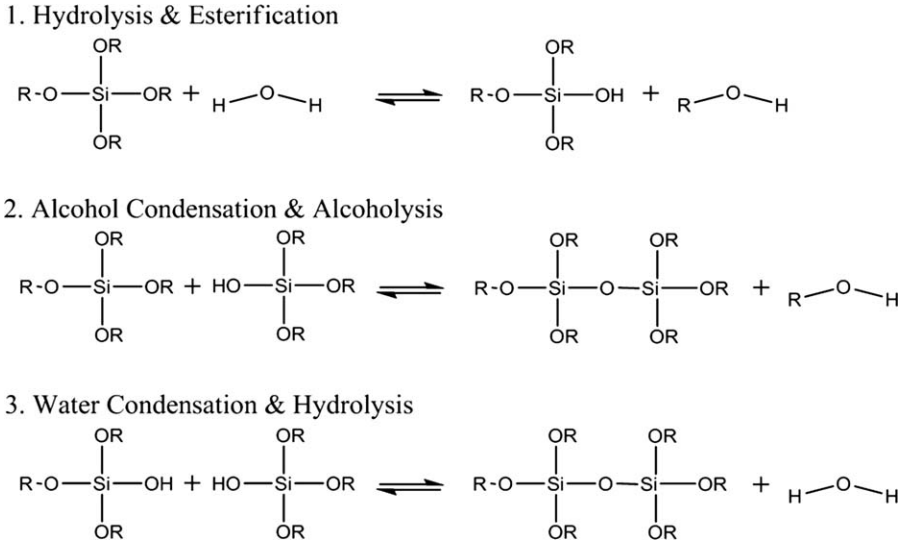

Figure 2 Sol–gel reactions with silicon alkoxide: (1) hydrolysis and (2,3) condensation.

Elemental analysis was performed, and the results are shown in Table III. The values obtained in this analysis, which were almost the same as the theoretical data, confirmed the correct identities of the synthesized products.

Porous morphology

EDX spectroscopy was used to confirm the complete etching of TEOS from the polymer matrix. It revealed a complete absence of silicon in the cryogenically fractured surface of the porous sample [Fig. 3(c,d)]. In contrast, the sample that underwent the TEOS treatment before etching showed a distinct silicon peak at 1.8 keV. Representative SEM images of the pure, hybrid, and porous PIs are shown in Figure 5. The surfaces were fractured by 5 s of cryogenic freezing in liquid nitrogen. Throughout the pure sample, the fractured surface showed a homogeneous phase. Pores that were 0.8–1.2 μm in size were found for the sample prepared with 10% TEOS. They were homogeneously dispersed throughout the sample and led to close cells of a regular spherical shape. A similar morphology was found for the sample with 20% porosity, but the pore sizes were greater (1.5–3.0 μm). These scans showed that at higher TEOS concentrations, larger pores were formed with a lower density. This might have been due to the higher agglomeration effect between TEOS particles during the gelling process. The samples fabricated in this work displayed a generally monodispersed closed-cell pore morphology in terms of the size and pore density despite the use of different PIs. Rogers et al.[33] in their study of perfect alternating PI–polysiloxane copolymers showed a great tendency for the separation of the two polymer phases: one is an organic base, whereas the other is an inorganic base. Hence, we expected that in this system the inorganic polysiloxane structure would agglomerate in the PI matrix. Hedrick et al.[12] fabricated porous PIs from α-methyl styrene and a styrene-based copolymer with the thermally labile copolymer technique. In comparison, the porous morphology derived from this thermally labile copolymer appeared to consist of interconnected, nonspherical pores.[6,12]

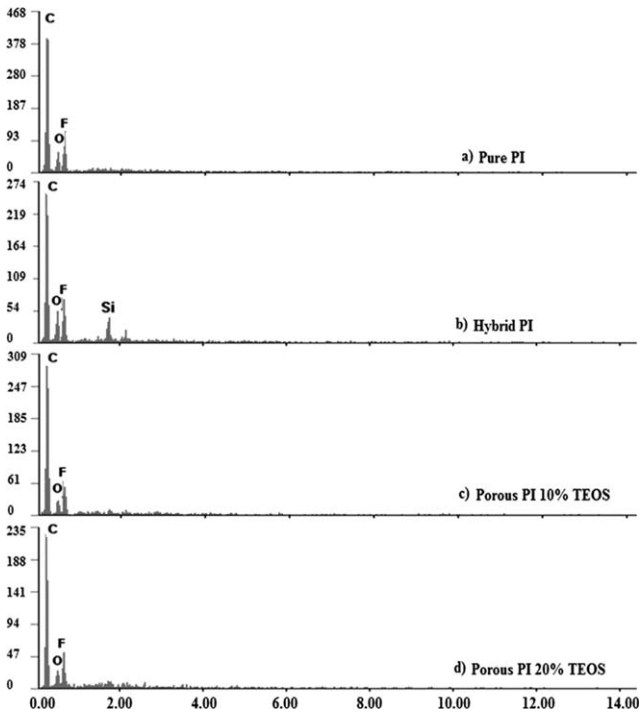

Figure 3 Chemical compositions of (a) the pure PI film, (b) the hybrid PI film, and (c,d) the PI/TEOS porous films (10 and 20 wt % TEOS, respectively) after etching according to EDX spectroscopy.

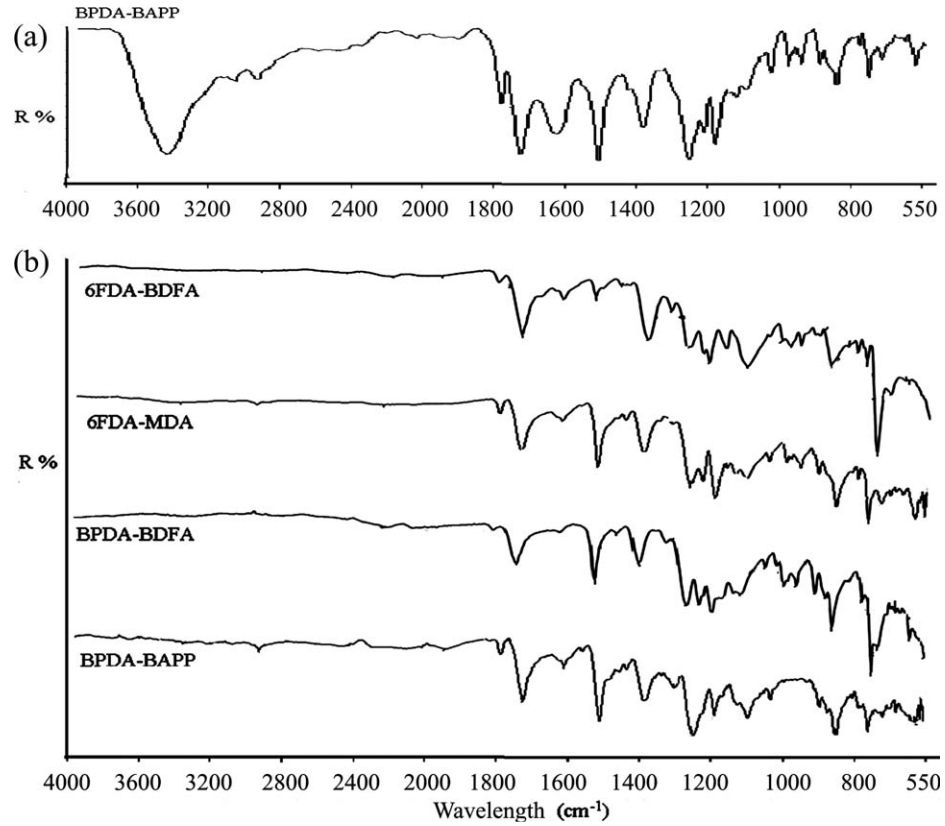

Figure 4 FTIR spectra confirming the identity of the products: (a) a representative spectrum of PAA and (b) spectra of the PI series.

Dielectric properties

The characteristic capacitance–voltage behavior of 6FDA–BDFA is shown in Figure 6, which displays the accumulation, depletion, and inversion regions. The film capacitance was taken to be the highest value in the accumulation region. The dielectric constant for the porous PI was calculated as follows:

$$C = \frac{\varepsilon_0 \varepsilon A}{t} \quad (1)$$

where C is the capacitance (F), ε is the dielectric constant (F/m), ε_0 is the initial dielectric constant (8.854×10^{-12} F/m), t is the film thickness, and A is the electrode surface area. The dielectric constants of the synthesized PIs are shown in Figure 7. Compared to the PI samples without the TEOS treatment, all the porous PIs fabricated in this work exhibited a significant decrease in the dielectric constant. The amount of the decrease corresponded well to the increase in the TEOS concentration. According to Jiang et al.,[3] the dielectric constant of a PI film is dependent on the intrinsic dielectric constant and the morphology of the porous structure.[3] Pores introduce air, the intrinsic dielectric constant of which is 1.0. This implies that the dielectric constant will proportionately decrease with an increase in the pore density. As shown in the SEM micrographs, the TEOS treatment generated a porous morphology. This explanation is well corroborated by the results obtained here (Figure 7). The sample with the 10% TEOS

TABLE III
Elemental Compositions of the Synthesized PIs

PI	Repeated unit formula (molecular weight)		C (%)	H (%)	N (%)
6FDA–BDFA	$C_{46}H_{22}F_{12}N_2O_6$ (926.12)	Calculated	77.00	3.07	3.91
		Found	75.89	2.95	3.85
6FDA–MDA	$C_{32}H_{16}F_6N_2O_4$ (606.10)	Calculated	63.38	2.64	4.62
		Found	64.56	2.32	4.48
BPDA–BDFA	$C_{43}H_{22}F_6N_2O_6$ (776.14)	Calculated	66.50	2.86	3.61
		Found	66.05	2.59	3.60
BPDA–BAPP	$C_{43}H_{28}N_2O_6$ (668.19)	Calculated	79.14	4.29	4.30
		Found	78.12	4.02	4.17

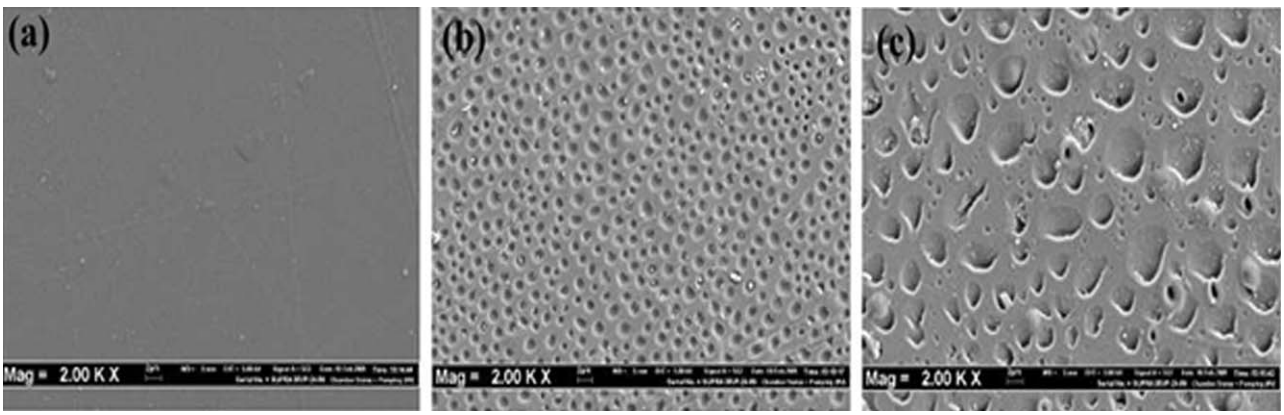

Figure 5 SEM images of the fracture surfaces of (a) pure PI, (b) porous PI/SiO_2 (10%), and (c) porous PI/SiO_2 (20%).

treatment had smaller pores despite a higher density, whereas the sample with the 20% TEOS treatment had bigger pores with a reduced density. The fact that the latter had a lower dielectric constant implies a higher porosity in comparison with the former. There was a reduction in the rate of the decrease in the dielectric constant as the TEOS concentration was increased from 10 to 20%. This could have been due to a tradeoff between the effects of the pore density and the overall void content in the polymer structures.

The relationship of the fluorine content and the dielectric constant is shown in Figure 8. There was a proportionate decrease in the dielectric constant as the weight percentage of fluorine in the structures increased because of the low polarizability of the fluorine atom (this low polarizability is due to its high electronegativity: the electrons are very tightly held and are close to the nucleus). This result reduced the ability of the electronic density in this region to align with the fluctuating electric field. Of the four synthesized PIs, BAPP–BPDA with no substituted fluorine had the highest dielectric constant. Therefore, the effect of polarizability was minimal. The other three PIs with substituted fluorines displayed decreases in the dielectric constant as expected. Simpson and St. Clair[17] concluded that the presence of fluorine increases the free volume, lowers electronic polarization, and can either increase or decrease the dielectric constant; the dielectric constant depends on whether the substitution of the atoms is symmetric or asymmetric. Symmetric substitutions of fluorine effectively induce a zero net dipole moment along the chain backbone. The substitution of fluorines in the synthesized PIs of this work was designed to be symmetrical to optimize the reductive effect on the dielectric constant. 6FDA–BDFA contained two trifluoromethyl groups symmetrically substituted at both the aniline and anhydride moieties. The dipole moments should have effectively canceled each other.

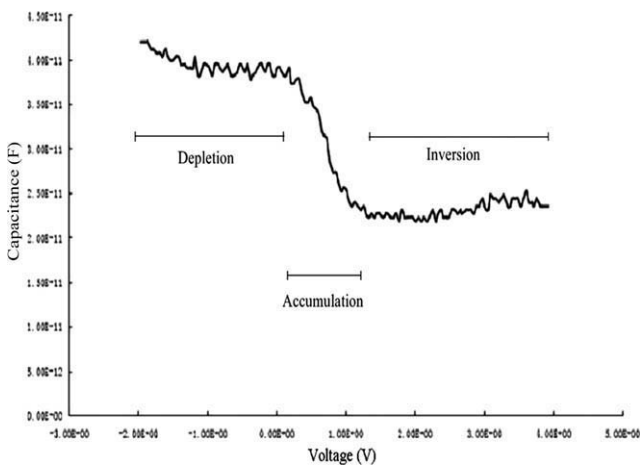

Figure 6 Characteristic capacitance–voltage plot (p-type) for porous 6FDA–BDFA.

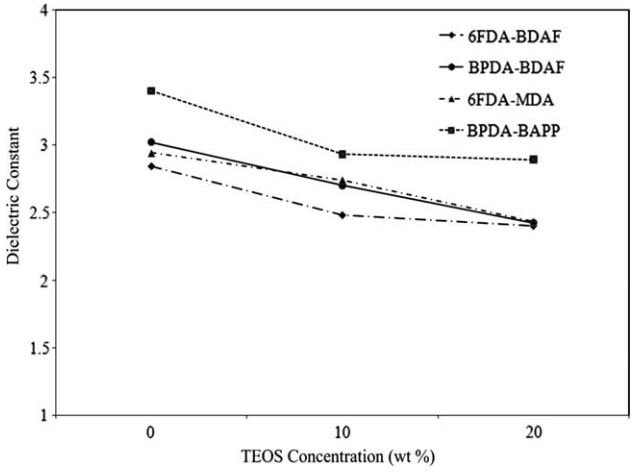

Figure 7 Relationship between the TEOS fraction and the dielectric constant at 1 MHz.

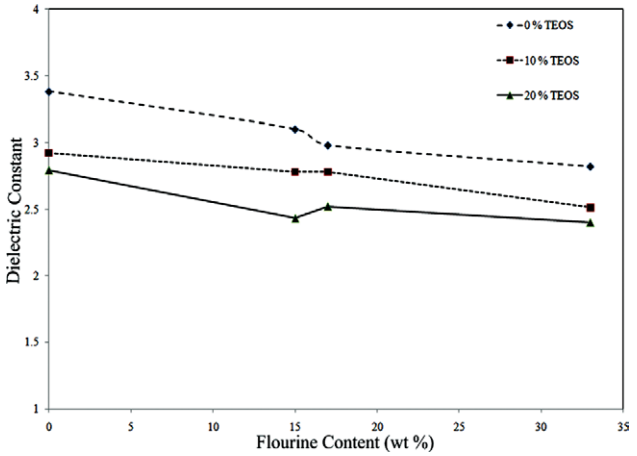

Figure 8 Relationship between the dielectric constant at 1 MHz and the fluorine content. [Color figure can be viewed in the online issue, which is available at wileyonlinelibrary.com.]

This configuration resulted in a large decrease in the dielectric constant. 6FDA–MDA and BPDA–BDFA contained two trifluoromethyl substituents at the anhydride and aniline moieties, respectively. Correspondingly, they had lower dielectric constants. According to Hougham et al.,[19] approximately 50% of the dielectric constant reduction is due to an increase in the free volume. The free volume is estimated as the difference between the occupied molar volume of the repeat unit and the total molar volume of the repeat unit. The atomic radius in the covalent bond for fluorine (0.72 Å) is far bigger than that for hydrogen (0.037 Å).[34] This implies that with the greatest fluorine content, the polarizability groups per unit of volume will be reduced.[17,20,35–37] Thus, the incorporation of a bulky trifluoromethyl substituent prevented the close packing of the polymer chains and effectively increased the free volume.[35–37] The porous PIs had lower dielectric constants at the cost of hardness. In the case of 6FDA–BDFA and 6FDA–MDA, there were reductions of 6.2% and 23.2%, respectively, in the hardness. These decreases were expected because of the presence of voids that loosened the structural framework and led to the inability of the polymers to withstand deformation.

The incorporation of fluorine into the PI chain backbone and the induction of porosity in this work further substantiate the viability of these strategies in reducing the dielectric constant of PIs. However, it is vital to note that the indiscriminate choice of PIs whose thermal properties are extreme will limit the range of their applications because of their intractability and difficult processing. The PIs synthesized in this work had moderate thermal properties, so these drawbacks could be overcome. Porosity induces a reduction of mechanical properties. In the future, we will try to balance the porosity and hardness to make these PIs viable for a wider range of applications.

CONCLUSIONS

Four PIs with different fluorine contents and porosity levels were successfully synthesized. They showed decreases in the dielectric constant with increased fluorine contents and porosity levels. The pore morphology had a high level of homogeneity in terms of density, size, and shape. These polymers possessed moderate thermal stability because of the presence of flexible bridging units. This could allow a favorable processing window for fabricating these polymers for thermally sensitive electronic applications.

References

1. Muruganand, S.; Narayandass, S.; Mangalaraj, D.; Vijayan, T. Polym Int 2001, 50, 1089.
2. Martin, S.; Godschalx, J.; Mills, M.; Shaffer, E., II; Townsend, P. Adv Mater 2000, 12, 1769.
3. Jiang, L.; Liu, J.; Wu, D.; Li, H.; Jin, R. Thin Solid Films 2006, 510, 241.
4. Park, S.; Cho, K.; Kim, S. J Colloid Interface Sci 2004, 272, 384.
5. Deligöz, H.; Yalcinyuva, T.; Özgümüs, S.; Yildirim, S. Eur Polym J 2006, 42, 1370.
6. Hedrick, J.; Carter, K.; Cha, H.; Hawker, C.; DiPietro, R.; Labadie, J.; Miller, R.; Russell, T.; Sanchez, M.; Volksen, W. React Funct Polym 1996, 30, 43.
7. Ahn, K.; Forbes, L. US Patent number 7285196 (2010).
8. Morgen, M.; Ryan, E.T.; Zhao, J.-H.; Hu, C.; Cho, T.; Ho, P.S., Ann Rev Mat Sci 2000, 30, 645.
9. Maier, G. Prog Polym Sci 2001, 26, 3.
10. Ghosh, M.; Mittal, K. Polyimides: Fundamentals and Applications; CRC: Boca Raton, FL, 1996.
11. Kuntman, A.; Kuntman, H. Microelectron J 2000, 31, 629.
12. Hedrick, J.; Carter, K.; Labadie, J.; Miller, R.; Volksen, W.; Hawker, C.; Yoon, D.; Russell, T.; McGrath, J.; Briber, R. Prog Polyimide Chem II 1999, 140, 1.
13. Hedrick, J.; Hawker, C.; DiPietro, R.; Jérôme, R.; Charlier, Y. Polymer 1995, 36, 4855.
14. Miyata, S.; Yoshida, K.; Shirokura, H.; Kashio, M.; Nagai, K. Polym Int 2009, 58, 1148.
15. Dhara, M. G.; Banerjee, S. Prog Polym Sci 2010, 35, 1022.
16. Carter, K.; DiPietro, R.; Sanchez, M.; Swanson, S. Chem Mater 2001, 13, 213.
17. Simpson, J.; St. Clair, A. Thin Solid Films 1997, 308, 480.
18. Alegaonkar, P.; Mandale, A.; Sainkar, S.; Bhoraskar, V. Nucl Instrum Methods Phys Res Sect B 2002, 194, 281.
19. Hougham, G.; Tesoro, G.; Viehbeck, A. Macromolecules 1996, 29, 3453.
20. Clair, A.; Clair, T.; Winfree, W. US Patent number 5338826 (1994).
21. Debye, P. Polar Molecules; Dover: New York, 1945.
22. Ahmad, Z.; Mark, J. Chem Mater 2001, 13, 3320.
23. Wen, J.; Wilkes, G. Chem Mater 1996, 8, 1667.

24. Sanchez, C.; Ribot, F. New J Chem 1994, 18, 1007.
25. Sanchez, C.; Ribot, F.; Lebeau, B. J Mater Chem 1999, 9, 35.
26. Cornelius, C.; Marand, E. Polymer 2002, 43, 2385.
27. Mittal, K. Polyimides: Synthesis, characterization, and applications. Volumes 1 & 2; Plenum Press: New York, 1984.
28. Giesa, R.; Keller, U.; Eiselt, P.; Schmidt, H. J Polym Sci Part A: Polym Chem 1993, 31, 141.
29. Chen, K.; Wang, T.; King, J.; Hung, A. J Appl Polym Sci 1993, 48, 291.
30. Kim, S. Macromolecules 2000, 33, 3190.
31. Yigit, M.; Seckin, T.; Koytepe, S.; Cetinkaya, E. Turk J Chem 2007, 31, 113.
32. Amutha, N.; Sarojadevi, M. J Appl Polym Sci 2008, 110, 1905.
33. Rogers, M. E.; Glass, T. E.; Mecham, S. J.; Rodrigues, D.; Wilkes, G. L.; McGrath, J. E. J Polym Sci Part A: Polym Chem 1994, 32, 2663.
34. Bondi, A. J Phys Chem 1964, 68, 441.
35. Liu, Y.; Xing, Y.; Zhang, Y.; Guan, S.; Zhang, H.; Wang, Y.; Jiang, Z. J Polym Sci Part A: Polym Chem 2010, 48, 3281.
36. Pan, H.; Pu, H.; Jin, M.; Wan, D.; Chang, Z. Polymer 2010, 51, 2305.
37. Jiang, X.; Gu, J.; Shen, Y.; Wang, S.; Tian, X. Desalination 2011, 265, 74.